Effects of Volute Curvature on Performance of a Low Specific-Speed Centrifugal Pump at Design and Off-Design Conditions

Article *in* Journal of Turbomachinery · April 2015

DOI: 10.1115/1.4028766

CITATIONS
45

READS
5,833

4 authors, including:

Hamed Alemi
University of Tehran
6 PUBLICATIONS **115** CITATIONS

SEE PROFILE

Mehrdad Raisee Dehkordi
University of Tehran
150 PUBLICATIONS **2,214** CITATIONS

SEE PROFILE

Amir Najafi
University of Tehran
31 PUBLICATIONS **494** CITATIONS

SEE PROFILE

Hamed Alemi[1]
Hydraulic Machinery Research Institute,
School of Mechanical Engineering,
College of Engineering,
University of Tehran,
Tehran 1439955961, Iran
e-mail: halemi@ut.ac.ir

Seyyed Ahmad Nourbakhsh
Hydraulic Machinery Research Institute,
School of Mechanical Engineering,
College of Engineering,
University of Tehran,
Tehran 1439955961, Iran
e-mail: anour@ut.ac.ir

Mehrdad Raisee
Hydraulic Machinery Research Institute,
School of Mechanical Engineering,
College of Engineering,
University of Tehran,
Tehran 1439955961, Iran
e-mail: mraisee@ut.ac.ir

Amir Farhad Najafi
Hydraulic Machinery Research Institute,
School of Mechanical Engineering,
College of Engineering,
University of Tehran,
Tehran 1439955961, Iran
e-mail: afnajafi@ut.ac.ir

Effects of Volute Curvature on Performance of a Low Specific-Speed Centrifugal Pump at Design and Off-Design Conditions

The effects of the volute geometry on the head, efficiency, and radial force of a low specific-speed centrifugal pump were investigated focusing on off-design conditions. This paper is divided into three parts. In the first part, the three-dimensional flow inside the pump with rectangular volute was simulated using three well-known turbulence models. Simulation results were compared with the available experimental data, and an acceptable agreement was obtained. In the second part, two volute design methods, namely, the constant velocity and the constant angular momentum were investigated. Obtained results showed that in general the constant velocity method gives more satisfactory performance. In the third part, three volutes with different cross section and diffuser shape were designed. In general, it was found that circular cross section volute with radial diffuser provides higher head and efficiency. Moreover, the minimum radial force occurs at higher flowrate in circular volute geometry comparing to rectangular cross section volute. [DOI: 10.1115/1.4028766]

Keywords: low-specific speed pump, CFD, radial force, velocity constant, diffuser shape, volute cross section

1 Introduction

The volute of centrifugal pumps is generally designed for an optimum or normal flowrate condition. In this case, the angular distribution of the static pressure round the impeller becomes approximately uniform. So, the lowest radial load is generated in normal condition. When pump is operating at off-design condition, impeller outflow does not match the volute geometry, and as a result, a nonuniform angular pressure distribution is established, resulting in radial force. Large radial force causes several troubles in pump such as: noise, vibration, and extra load on the bearings. To reduce such undesirable effects, during the last years, a number of researchers have investigated the effects of geometrical parameters on the radial force in centrifugal pumps. The internal flow developing in a pump at off-design conditions is extremely complex due to blade curvatures, impeller rotation, rotor–stator interaction, turbulence effects, and flow separation. Therefore, in numerical study, it is necessary to employ reliable turbulence models with accurate numerical methods for prediction of complex flow in centrifugal pumps. During recent years, numerous studies have been conducted to apply computational fluid dynamics (CFD) methods for the simulation of turbulent flow in centrifugal pumps. In the following some of these investigations are briefly reviewed. Gulich and Favre [1] carried out the numerical calculation for various impellers with specific speeds ranging from $N_s = 12$ to 160 using a commercial CFD code and compared the numerical results with the experimental data. They showed that the pump head could be estimated with a standard deviation of 2.5% by CFD simulation using the standard k-ε turbulence model. Kelder et al. [2] studied turbulent flow at Reynolds number of 1.7×10^6 in the volute of a low specific-speed pump both experimentally and numerically close to the design point. They showed that in this condition, the core flow behaves like a potential flow. Thus, they employed inviscid equations to solve flow field. Feng et al. [3] applied various turbulence models to simulate nonstationary turbulent flow in a radial diffuser pump. The numerical results obtained for the pressure, velocity, and turbulence fields were analyzed and compared with laser Doppler velocimetry (LDV) and particle image velocimetry (PIV) data. They reported that the choice of turbulence model does not have a significant influence on the pressure field. Among all turbulence models, the k-ω turbulence model had superior performance on prediction of the velocity vector directions as well as the turbulent kinetic energy levels. Cheah et al. [4] simulated the 3D and nonstationary turbulent flow through the centrifugal pump by means of commercial CFX 11.0 code, using the standard k-ε turbulence model with scalable log-law wall functions for wall boundary condition treatment. Their numerical results predicted the head coefficient in good agreement with the experimental data. They observed that flow separation occurs at the impeller leading edge due to nontangential inflow conditions as caused by the inlet curved duct. Gonzalez et al. [5] presented a comparison between numerical simulations and experiments to examine the effectiveness of CFD method in capturing pressure pulsation for a wide range of flowrates inside a centrifugal pump. They obtained the amplitude of the fluctuating pressure field by means of CFD simulation using the standard k-ε turbulence model. Spence and Amaral-Teixeira [6] studied experimentally and numerically the effect of four geometric parameters, namely, cut-water gap, vane arrangement, snubber gap, and the side wall clearance on the pressure pulsation within a complete double entry, double volute

[1]Corresponding author.

Contributed by the Heat Transfer Division of ASME for publication in the JOURNAL OF TURBOMACHINERY. Manuscript received November 29, 2013; final manuscript received September 30, 2014; published online November 26, 2014. Assoc. Editor: Stephen W. T. Spence.

centrifugal pump using multiblock, structured grid, and TASC-flow CFD code. Finally, they recommended proper values for all parameters to reduce pressure fluctuation and radial force. Jafarzadeh et al. [7] studied turbulent flow within a low-N_s, high-speed centrifugal pump, using three dimensional numerical simulation and the k-ε turbulence model. They investigated the effect of number of blades on the efficiency of pump and found that the position of blades with respect to the tongue has a great influence on the separation. Yang et al. [8] investigated the effects of various volute geometries by means of ANSYS-CFX software using the standard RNG k-ε turbulence model in a pump with $N_s = 23$. Their research showed that volute with round cross section gives more head and efficiency in comparison with trapezoidal and rectangular cross sections. More recently, Torabi and Nourbakhsh [9] studied the effects of some volutes geometrical factor variation on radial force. They found that the gap between impeller and tongue severely affects the radial force. More specifically, they found that 6% reduction in the gap increases the maximum value of the static pressure by 50% round the impeller exit.

As mentioned above, a number of experimental and numerical investigations have been performed to study the effects of various geometrical parameters on the hydraulic performance and radial force of centrifugal pumps. However, almost none of the previous investigations studied numerically the influence of main geometrical parameters of volute curvature including velocity or angular momentum constant method design, cross section shape, and outlet diffuser shape on pump performance and radial force in a comprehensive way. In order to fill this gap, in the first part, numerical simulation was validated using available experimental data. In the second part two methods of volute design, namely, velocity constant and angular momentum constant were compared. Finally, in the third part, the effects of cross section shape, and outlet diffuser shape on hydraulic characteristics of a centrifugal pump were investigated.

2 Main Pump Parameters

In this study, experimental measurement of Kelder et al. [2] was used for CFD validation. Design conditions of the studied pump are summarized in Table 1. The details of pump geometry used by Kelder et al. [2] are shown in Fig. 1. The investigated centrifugal pumps have a low-N_s of 21. The impeller consists of seven blades with a constant blade angle of 70 deg with respect to the radial direction and a constant blade thickness of 2 mm. The main volute possesses a compound cross section. As shown in Fig. 1(*b*), this compound is made of rectangle and trapezoid cross sections. The volute tongue has a cylindrical shape with a diameter of 2 mm. Experiments were performed at flowrates of 82.5%, 100%, and 112% of the normal flowrate. LDV measurement system was used for velocity measurements. In addition, static pressure detection was performed using U-tube manometers. Velocity and static pressure data were collected at the locations shown in Fig. 1. As shown in Fig. 1, the pressure tabs are located at the shroud side just outside the impeller and at mid-height of outer wall in volute. More details of pump configuration and experimental method can be found in Kelder et al. [2].

3 Numerical Method and Model Description

In this study, a commercial code was used to solve the full 3D Reynolds-averaged Navier–Stokes (3D-RANS) equations for different working conditions. The governing equations are presented in the Appendix. The solver is a 3D CFD code in which the governing equations are discretized using the finite-element based finite-volume method. Two main advantages of such hybrid CFD method are geometric flexibility due to the finite-element method and retaining the conservation properties of the finite-volume method. That results in low numerical error on nonsmooth grids. The second-order upwind scheme was applied for the space discretization. For grid generation, the 3D models of impellers and volute were first generated, and then exported to commercial software. Water at 25 °C was selected as the working fluid. For boundary conditions, a constant mass flowrate and normal flow direction was applied at the inlet while a constant pressure was specified at the outlet. Spence and Amaral-Texeira [10] reported that these boundary conditions cause rapid convergence.

Table 1 Main parameters of pump

Parameter	Value
Metric specific speed, N_s	21
Nominal flow coefficient, ϕ_n	0.15
Nominal head coefficient, ψ_n	0.124
Impeller exit diameter, d_2 (mm)	640
Impeller exit width, b_2 (mm)	25
Number of blades, Z	7

It was found that by increasing the turbulent intensity at inlet from 5% to 10% and viscosity ratio from 10 to 100, the predicted head changes less than 0.01%. So, turbulent intensity and viscosity ratio were set to be 5% and 10%, respectively. The convergence criteria for numerical simulation were set at maximum residuals of 1×10^{-4}.

For mesh generation, at first the pump was split into four components. As shown in Fig. 2(*a*), the components are: (i) inlet duct, (ii) impeller, (iii) volute, and (iv) outlet duct. Straight duct at inlet and outlet were used to prevent boundary condition effects on simulation of the pump flow domain.

Each module has been meshed independently. Figure 2(*b*) shows the generated grids for the pump impeller and volute. Due to complexity of geometry, the hexahedral (near walls) and tetrahedral cells were used for inlet and outlet modules, and tetrahedral cells were used for impeller and volute. Close to some important regions, such as the leading and trailing edge of the blades and the volute tongue where flow separation may occur, mesh clustering was applied (see Fig. 2). In grid generation process, orthogonal quality, aspect ratio, and skewness were assured to be in desirable range. For steady simulation the grids between the impeller and volute in one hand, and inlet duct and impeller on the other hand, are conjoined by means of a frozen rotor interface. In other words, for steady simulation, impeller rotation is considered and the frame of reference is changed but the relative orientation of the components across the interface is fixed. Both two frames of reference connect in such a way that each of them has a fixed relative position throughout the calculation. This is equivalent to taking a snapshot from the flow field in an instance of time. Moreover, general grid interface was employed between volute and outlet duct.

Grid independency studies were performed using different mesh sizes. Figure 3 shows head coefficient normalized by experimental head coefficient versus mesh size. It was found that by increasing the number of cells from 7.3×10^5 to 1.2×10^6 changes in the predicted head is about 0.8%. Further mesh refinement from 1.2×10^6 cells to 1.9×10^6 decreases the head by about 0.7%. Since the predicted head does not show a great sensitivity to the grid refinement, the numerical results can be considered as grid independent. All the numerical results were obtained using the mesh with 1.2×10^6 cells due to having more confidence in achievement.

4 Results

4.1 Numerical Simulation of Flow Through Main Pump. The numerical simulations of the present study were validated by comparing the predicted static pressure and velocity components with the experimental data [2] at selected locations. As shown in Fig. 1, the static pressure was measured at the impeller periphery and volute center wall, while velocity data were obtained in a plane located at the center of the volute. In this paper, three well-known turbulence models were examined; namely, the standard k-ε, the low-Re k-ω, and the shear stress transport (SST). These

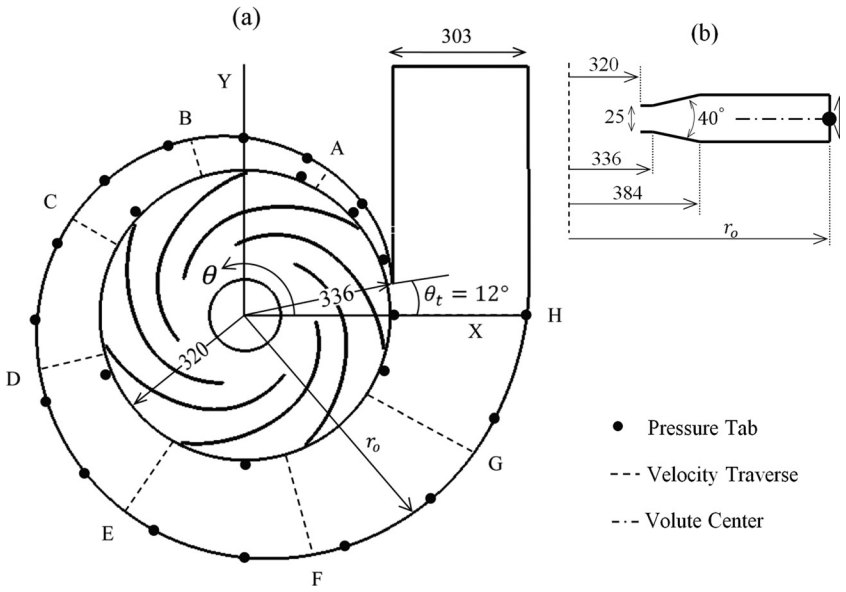

Fig. 1 (*a*) Kelder volute geometry and locations of velocity and static pressure measurement. (*b*) Volute cross section dimensions in millimeters.

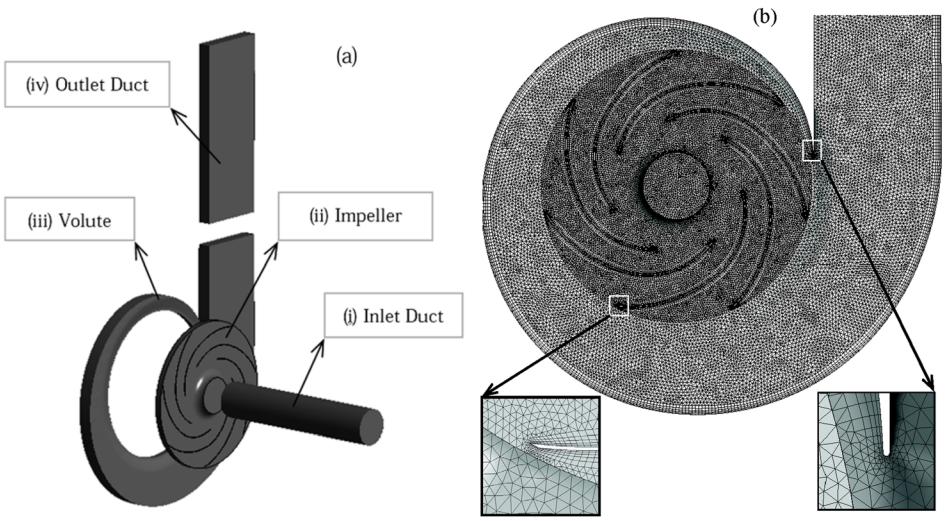

Fig. 2 (*a*) 3D models of total domain including (i) inlet duct, (ii) impeller, (iii) volute, and (iv) outlet duct; (*b*) computational mesh for the investigated pump

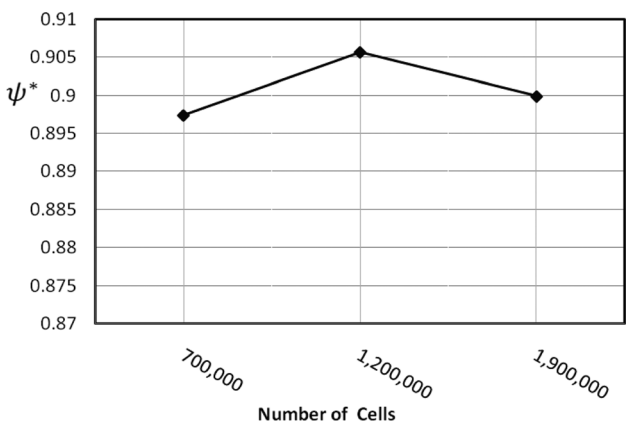

Fig. 3 Head coefficient versus mesh size

turbulence models are described in the Appendix. In Fig. 4, pressure distributions obtained from three turbulence models are compared with the experimental data [2]. Experimental and numerical results showed that depending on the value of flowrate, the static pressure distribution has different behavior. For the design flowrate, the static pressure remains almost uniform which leads to minimum radial force. At the off-design condition corresponding to the low capacity $\phi/\phi_n = 0.825$, the static pressure increases with θ while an opposite trend is observed for $\phi/\phi_n = 1.12$. The wavy shape of pressure distribution can be seen in CFD predictions; that is due to impeller blades effects. It is seen that all three turbulence models give comparable results in both design and off-design conditions. Despite the presence of local discrepancies between CFD predictions and measurements, both the level and trend of CFD results are in overall agreement with the measurements.

In Fig. 5, the predicted radial and tangential velocity components are compared with the experimental data of Kelder et al. [2]. Comparisons were made for three working conditions ($\phi/\phi_n = 0.825$, 1.0, and 1.12) along four traverse sections (A, D, F, and

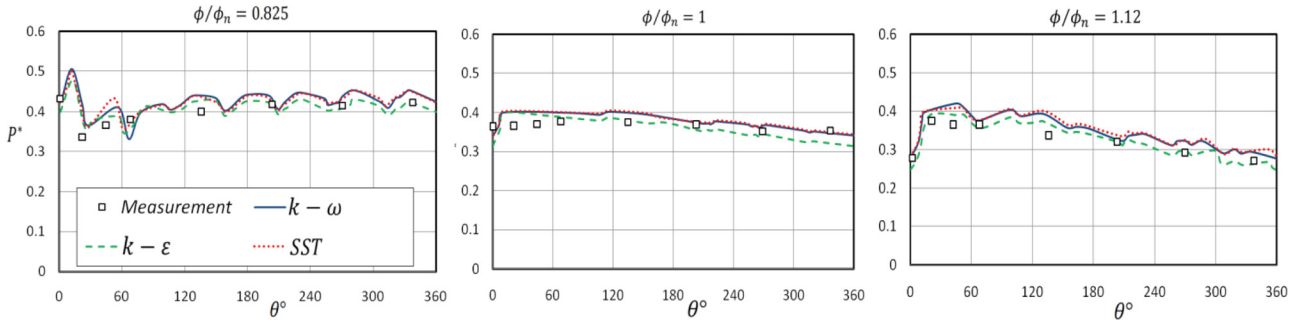

Fig. 4 The pressure distributions of impeller periphery

H) of the volute (see Fig. 1). However, some discrepancies between turbulence models at $\phi/\phi_n = 0.825$ are seen here, again all turbulence models returned similar results consistent with the experimental data of Kelder et al. [2]. It should be noted that discrepancies between computations and experimental data could be partly due to the uncertainties in measurements. An uncertainty analysis gives a relative uncertainty of about 3% in pressure and head.

As mentioned in the Introduction, Kelder et al. [2] employed Euler equation in their numerical predictions and found reasonable agreement between computational and experimental data. However, level of agreement was not as good as those shown in Fig. 5. For instance, at $\phi/\phi_n = 0.825$ on traverse A, RMS error of present CFD results is about 11% whereas it is about 25% for Kelder results [2].

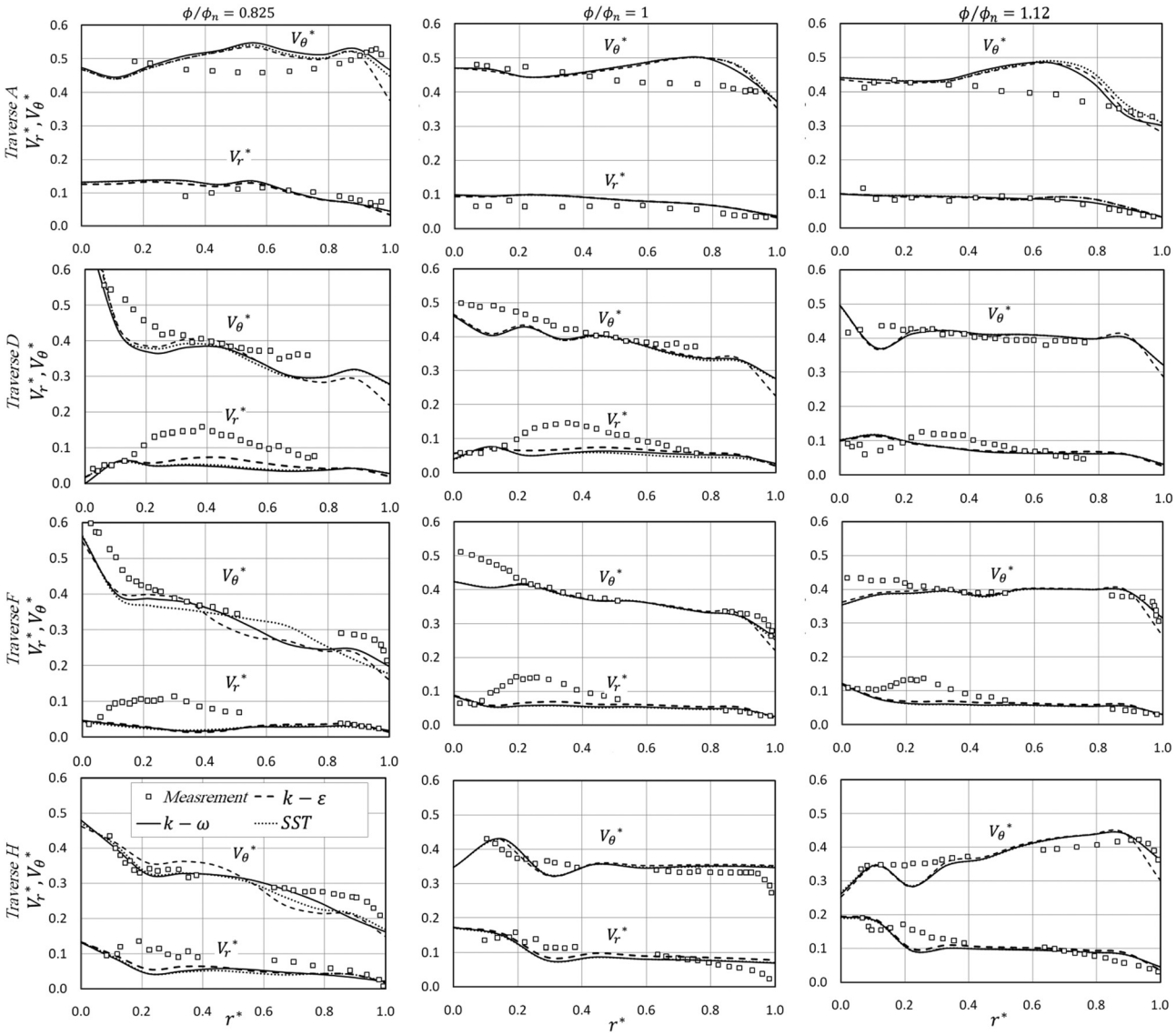

Fig. 5 Comparison of predicted and measured nondimensional radial and circumferential velocities in the volute along different traverses in $\phi/\phi_n = 0.825, 1,$ and 1.12

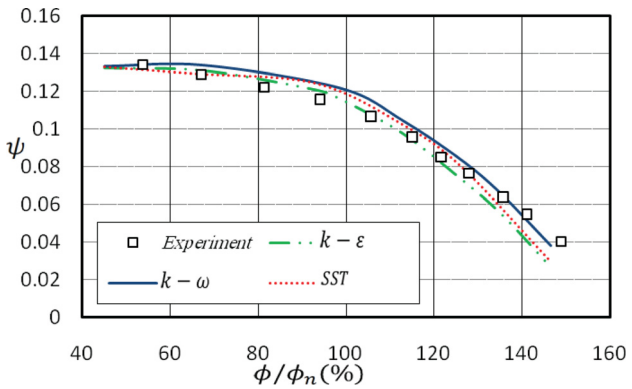

Fig. 6 Comparison of predicted head using various turbulence models with the experimental data

In Fig. 6, the predicted head coefficients using three turbulent models are compared with experimental data for a wide range of flow coefficients, including the design point and off-design conditions. Although the k-ε turbulence model returns more accurate results for the nondimensional head near the design point, the head predictions of the k-ω model at off-design conditions are closer to the experimental data especially at high flowrate. Since, the principal focus of current study was on off-design conditions, the k-ω turbulence model with automatic near wall treatments was employed for calculations.

When the position of blade with respect to tongue (θ) changes, pressure and velocity distribution in the volute vary due to interaction between the impeller blade and volute tongue. In other words, pump characteristics are instantaneous and unsteady. To study unsteadiness of flow regime, Fig. 7 presents pump performance curves versus blade location with respect to the tongue. The results indicate that when blades location vary with respect to

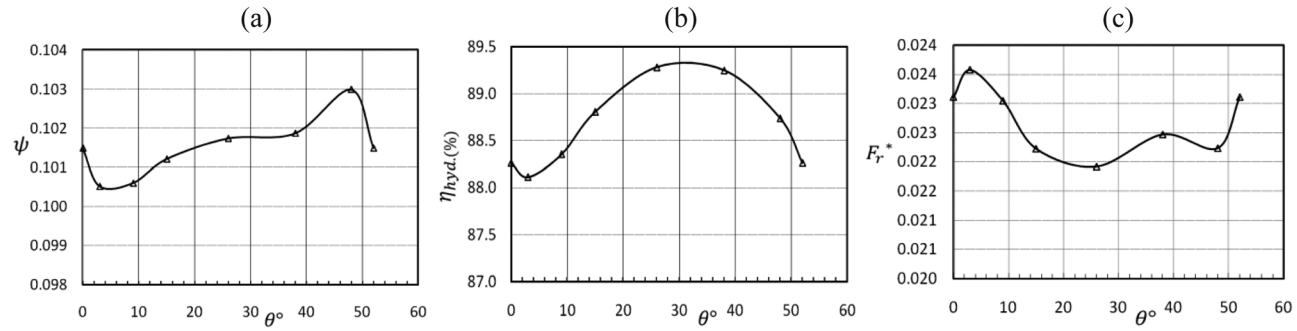

Fig. 7 Pump performance versus blade location with respect to tongue

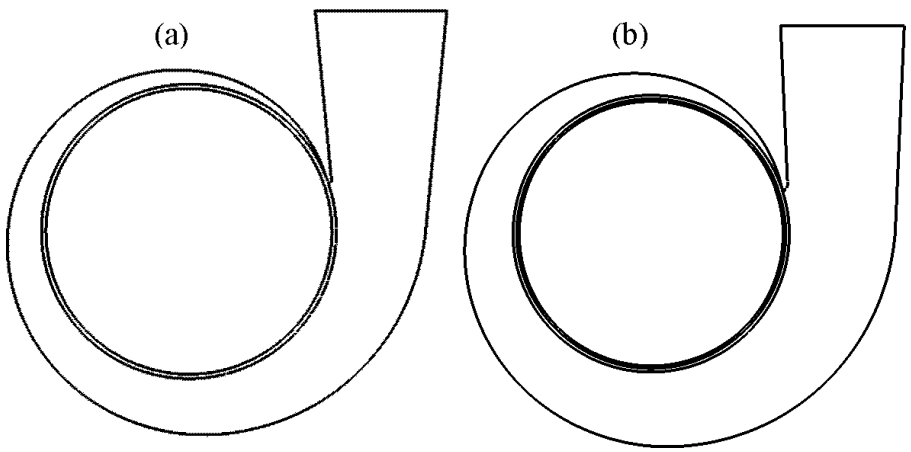

Fig. 8 2D models of volutes using (*a*) Pfleiderer design and (*b*) Stepanoff design

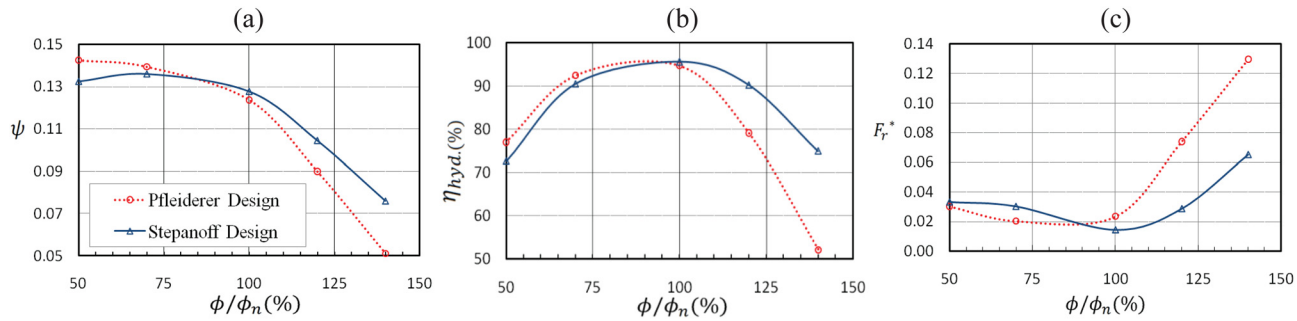

Fig. 9 Numerical results of volute pump using Pfleiderer, and Stepanoff methods for volute design

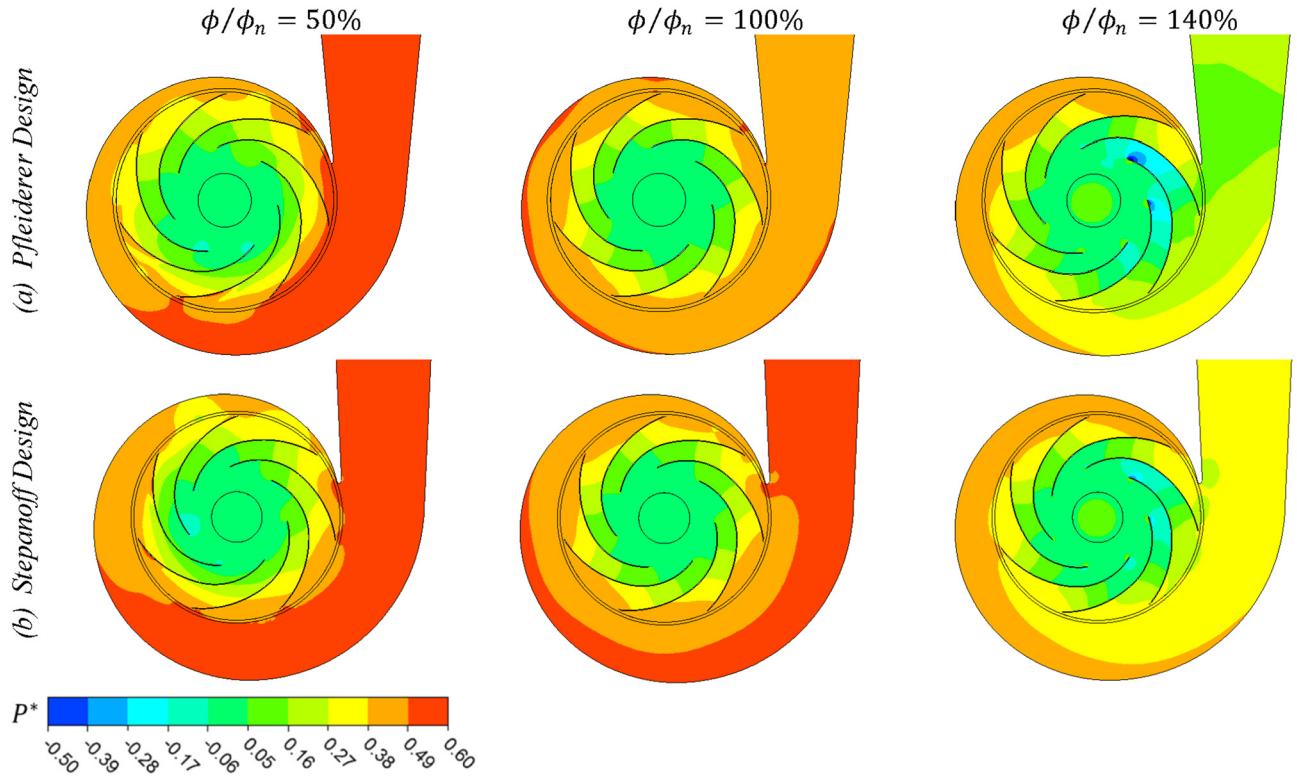

Fig. 10 Pressure contours for Pfleiderer and Stepanoff design

tongue, head magnitude, efficiency, and radial forces will alter less than 2.5%, 1.5%, and 8%, respectively. However, for quasi-steady simulation of present work, in all cases, the tongue was similarly located in the midposition of two blades ($\theta = 25.7$ deg).

4.2 Comparison of Velocity Constant and Angular Momentum Constant Methods Volute Design. The preliminary step for volute design is cross section area calculation. For this purpose, it is essential to select a circumferential velocity (C_u) distribution around impeller periphery in volute. C_u represents the tangential component of absolute velocity in the impeller outlet and circumferential velocity in volute. The difference of these two methods would be made obvious far from impeller outlet in volute where on every section C_u or rC_u should be remained constant. According to traditional design rules, two alternatives are available. First alternative, proposed by Stepanoff [11], assumes a constant tangential velocity. This design results in uniform theoretical

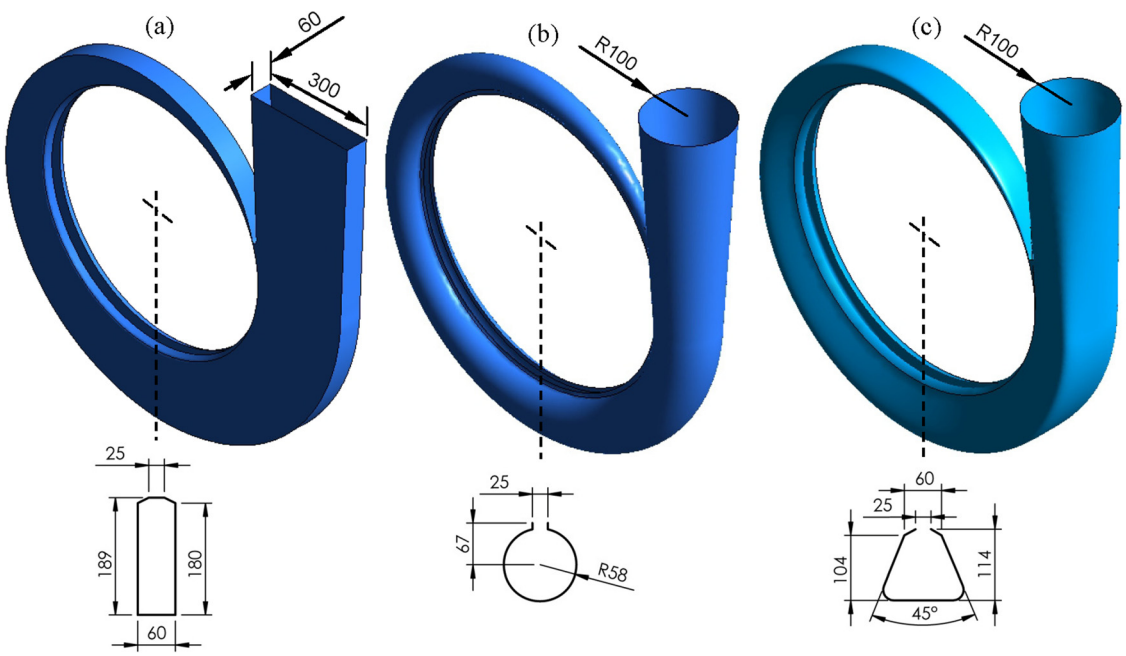

Fig. 11 3D models and cross section dimensional parameters (in millimeters) of (*a*) rectangular cross section, (*b*) circular cross section, and (*c*) trapezoidal cross section

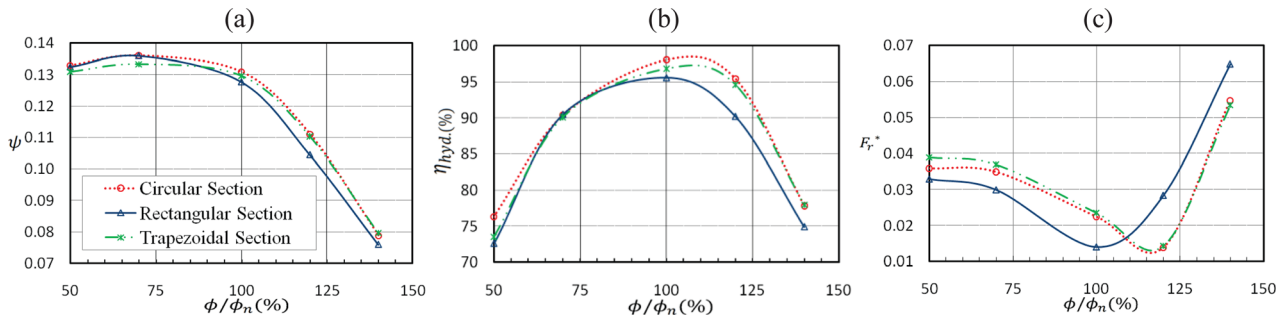

Fig. 12 Pump characteristics with different cross section shape

static pressure distribution around impeller periphery at design point. Second alternative proposed by Pfleiderer [12] takes constant angular moment, rC_u, in volute.

Due to circumferential velocity variation, it is expected that the uniformity of static pressure is deteriorated around impeller periphery at design point using this method. In this paper, two volutes are designed using the above mentioned methods. In Figs. 8(*a*) and 8(*b*), 2D models of two volutes are demonstrated. In both volutes outlet cross sections were kept the same. Figure 9 shows numerical results of two new designed volutes. As expected, the radial force of Stepanoff design at normal point is somewhat lower than the radial force of Pfleiderer design due to uniform pressure distribution round impeller periphery. Pfleiderer design produces a slightly higher head and efficiency in low capacity that is consistent with Yang et al. [8] reports. At high capacity, the Stepanoff design yields far better performance characteristics than the Pfleiderer design, and the radial force is much lower than that of the Pfleiderer design. Figure 10 clearly displays that pressure

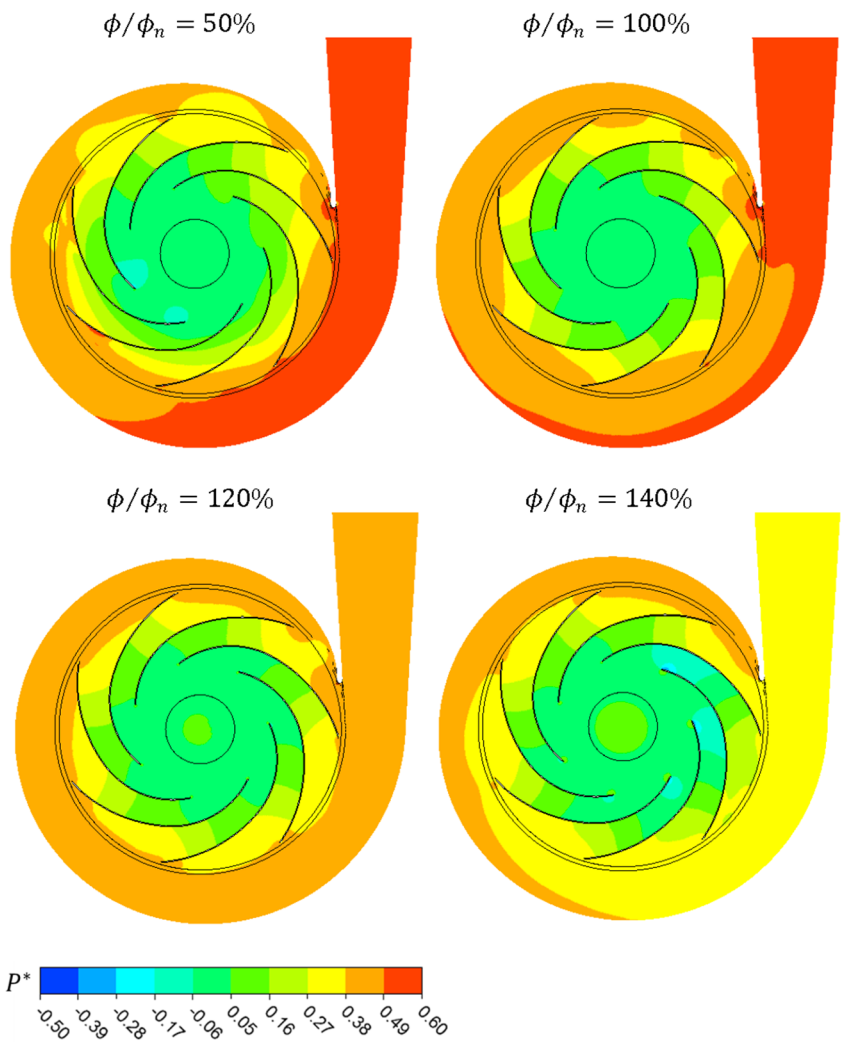

Fig. 13 Pressure contours in circular cross section volute

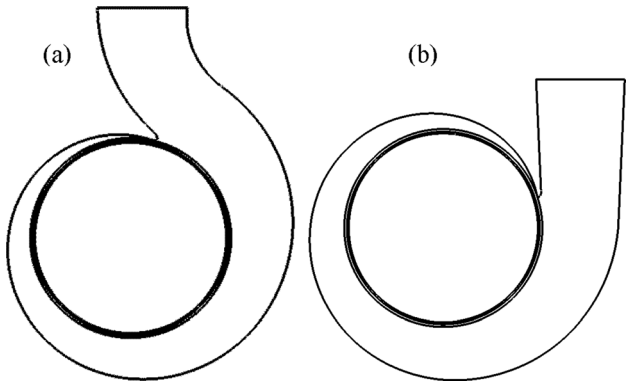

Fig. 14 2D views of (*a*) radial diffuser and (*b*) tangential diffuser

contour around impeller in Stepanoff design is much more uniform in high capacity and this results in lower radial force generation shown in Fig. 9(*c*). Another point of interest in Fig. 10 is the low pressure region near leading edge of blades located toward tongue due to dropping the local static pressure at $\phi/\phi_n = 140\%$. This region is extended more in Pfleiderer design that leads to higher possibility of cavitation. This means that the design criteria of the volute do not take into account the fact that the impeller has a not negligible interaction with the volute.

4.3 Design of Volutes With New Geometry

4.3.1 Design of Volutes With Different Cross Section Shapes. In this section, three new volutes with different cross section shapes, including rectangular, circular, and trapezoidal cross sections, were probed into (see Figs. 11(*a*)–11(*c*)). All three volutes were designed using velocity constant method; and cross-sectional areas of three designs are the same. Figure 12 demonstrates pump performances obtained from CFD simulation for corresponding cross sections. It is seen that circular cross section volute is the best considering head and efficiency. Yang et al. [8] reports similar results. However, circular and trapezoidal cross sections have higher radial force, at design point and low flowrate. At high flowrate, trapezoidal and circular volutes produce better condition. Hydraulic radii of circular and trapezoidal geometries are higher than rectangular one which causes reduction in pressure loss. An interesting matter to be noticed here is the shift of minimum radial force point of circular and trapezoidal cross section volutes to higher flowrate equal to about 115% Q_n of rectangular volute. As shown in Fig. 12(*b*), it could be due to higher efficiency and better flow regime of these volutes near 115% Q_n.

As displayed in Fig. 13, pressure distribution around impeller is the most uniform at $\phi/\phi_n = 120\%$ that is consistent with the lowest radial force shown in Fig. 11(*c*).

4.3.2 Design of Volute With Different Diffuser Shape. There are two alternatives for the selection of diffuser shape in volute design; namely, radial diffuser and tangential diffuser. In Figs. 14(*a*) and 14(*b*), 2D views of these diffusers are shown whereas the volute geometry is the same for two designs. Figure 15 shows the results obtained from CFD calculations. As can be seen, both diffusers provide more or less the same head but radial diffuser gives a slightly higher efficiency at design point and high flowrate. Also, radial diffuser produces lower radial force at design point and low flowrate.

5 Conclusion

In this paper, the hydraulic characteristics of a low-N_s centrifugal pump with various volutes were numerically investigated by means of commercial software. In the first part, CFD results of all turbulence models were found to be in reasonable agreement with the measurements. Based on the predictions, the k-ω turbulence model with automatic near wall treatments was chosen for further analysis. In total, five various volutes were designed to study the influence of various geometrical parameters on the head, efficiency, and radial force.

In the second part, it is found that Stepanoff design generates lower radial force than Pfleiderer design at normal flowrate. Also, Stepanoff design encompasses more appropriate condition in head, efficiency, and radial load in high flowrate, though the Pfleiderer design provides superior condition in low flowrate.

In the last part, results showed that the circular cross section volute provides higher head and efficiency than the other cross sections in almost entire flowrate. Trapezoidal and circular cross sections give lower radial force at high capacity rate while rectangular cross section yields lower radial force at low capacity rate. Another point of interest was shifting the minimum radial force point of circular and trapezoidal cross section volutes to higher flowrate about 115% Q_n of rectangular cross section volute. This means that the minimum radial force does not essentially occur at the best efficiency point depending on volute shape geometry. The volute with radial diffuser gave slightly more efficiency at normal and high flowrate comparing to the volute with tangential diffuser, also produced lower radial force at normal and low flowrate.

Finally, it can be concluded from the numerical results that generally, Stepanoff volute design with circular cross section and radial diffuser shape provides better hydraulic performance and lower radial force especially at high flowrate. In low-N_s pump, the generated radial force at high flowrate is significantly more than radial force at low capacity. This alarms that bearing selection based on zero-flow condition may be risky in low-N_s pumps.

Acknowledgment

The authors gratefully acknowledge the financial support of Hydraulic Machinery Research Institute, School of Mechanical Engineering, College of Engineering, University of Tehran.

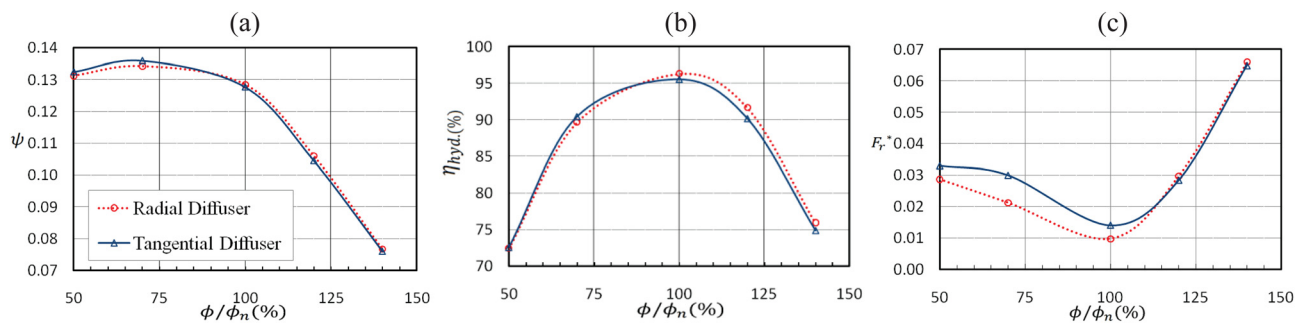

Fig. 15 Numerical simulation result for volutes with radial diffuser and tangential diffuser

Nomenclature

b_2 = breadth of impeller at discharge (mm)
C_u = circumferential or tangential velocity (m/s)
d_2 = outside diameter of impeller (mm)
F_r = radial force (N)
F_1, F_2 = blending functions
$F_r^* = F_r/(0.5\rho u_2^2 \pi d_2 b_2)$, radial force coefficient (nondimensional)
g = standard gravity acceleration (m/s^2)
H, H_n = head, normal or design head (m)
$k = \frac{1}{2}\left(\overline{u^2} + \overline{v^2} + \overline{w^2}\right)$, turbulent kinetic energy (m^2/s^2)
N = rotation speed (r/min)
$N_s = NQ^{0.5}H^{-0.75}$, metric specific speed (r/min, m^3/s, m)
P = static pressure (Pa)
P_{in} = inlet static pressure (Pa)
P_k = Production rate of the turbulent kinetic energy (m^2/ s^3)
$P^* = (P - P_{in})/\rho u_2^2$, pressure coefficient (nondimensional)
Q, Q_n = flowrate, Normal or design flowrate (m^3/s)
r_o = radius of volute wall midline (mm)
r_4 = volute inlet radius (mm)
$r^* = (r - r_4)/(r_o - r_4)$, volute radial distance (nondimensional)
Re $= (\Omega d_2^2)/\upsilon$, Reynolds number (nondimensional)
T_{ave} = average pressure and viscous moment on impeller walls (N · m)
$u_i = (u, v, w)$, fluctuating velocity vector in tensor notation (m/s)
$U_i = (U, V, W)$, mean velocity vector in tensor notation (m/s)
u_2 = blade tip velocity (m/s)
$u^+ = U/(\tau_w/\rho)^{0.5}$ (nondimensional)
$V_r^* = V_r/u_2$, radial velocity (nondimensional)
$V_\theta^* = V_\theta/u_2$, circumferential velocity (nondimensional)
$x_i = [X, Y, Z]$, Cartesian coordinates in tensor notation (m)
$y^+ = \exp[(u^+ - 5.5)/2.5]$ distance from the wall (nondimensional)
Z = number of blades

Greek Symbols

$C_\mu, C_{\varepsilon 1}, C_{\varepsilon 2}, \sigma_k, \sigma_\varepsilon$ = k-ε turbulence model coefficients
$\beta', \beta, \sigma_k, \sigma_\omega, \alpha$ = k-ω turbulence model coefficients
$\varepsilon = 2\upsilon \overline{\frac{\partial u_i}{\partial x_j}\frac{\partial u_i}{\partial x_j}}$, dissipation rate (m^2/s^3)
ε_{ijk} = permutation symbol
$\eta_{hyd} = \rho g Q H/(T_{ave}\Omega)$, hydraulic efficiency (%)
θ, θ_t = angular coordinate, angular position of tongue (deg)
ρ = fluid density (kg/m^3)
υ = kinematic viscosity (m^2/s)
υ_t = kinematic turbulent viscosity (m^2/s)
$\phi, \phi_n = Q/(\Omega d_2^2 b_2)$, flow coefficient, flow coefficient at normal flowrate Q_n (nondimensional)
$\psi, \psi_n = gH/(\Omega^2 d^2)$, head coefficient, head coefficient at normal head rate H_n (nondimensional)
ψ^* = normalized head coefficient by the head coefficient of experiment (nondimensional)
$\omega = k/\upsilon_t$, specific dissipation rate (1/s)
Ω = rotation speed or rotation vector (rad/s)

Appendix

A.1 Governing Equations

Since the flows in most engineering applications, including centrifugal pumps, are turbulent, the Navier–Stokes equations need to be averaged over a period of time longer than the time scale of flow applying the Reynolds decomposition, where flow quantities are decomposed in a mean and a fluctuating component. The application of this decomposition and subsequent time averaging results in RANS equations; where the turbulence effect appears as a second order tensor representing the interaction between the fluctuating velocities. RANS equations for statistically stationary flow can be written in the following way, as the continuity equation:

$$\frac{\partial U_j}{\partial x_j} = 0 \tag{A1}$$

and momentum equations as

$$\frac{\partial}{\partial x_j}(U_j U_i) = -\frac{1}{\rho}\frac{\partial P}{\partial x_i} + \frac{\partial}{\partial x_j}\left[\upsilon \frac{\partial U_i}{\partial x_j} - \overline{u_i u_j}\right] - 2\epsilon_{ijp}\Omega_p U_j - \left[\Omega_j X_j \Omega_i - \Omega_j X_i \Omega_j\right] \tag{A2}$$

where Ω denotes the rotation vector of the coordinate system and X the position vector. The first group of rotation terms represents the Coriolis forces and the second group the centrifugal forces. When a domain with a stationary frame is specified, Coriolis and centrifugal momentum terms vanished.

A.2 Turbulence Models

A.2.1 The Standard k-ε Turbulence Model. In k-ε turbulence model, the Reynolds stress tensor $-\rho\overline{u_i u_j}$ is obtained from the eddy-viscosity approximation

$$\overline{u_i u_j} = \frac{2}{3}\delta_{ij}k - \upsilon_t\left(\frac{\partial U_i}{\partial x_j} + \frac{\partial U_j}{\partial x_i}\right) \tag{A3}$$

where the kinematic turbulent viscosity, υ_t, is defined as

$$\upsilon_t = C_\mu \frac{k^2}{\varepsilon} \tag{A4}$$

To obtain υ_t, the following transport equations for the turbulence kinetic energy, k, and its dissipation rate,ε, are solved

$$\frac{\partial}{\partial x_j}(U_i k) = \frac{\partial}{\partial x_j}\left[\frac{\upsilon_t}{\sigma_k}\frac{\partial k}{\partial x_j}\right] + P_k\text{-}\varepsilon \tag{A5}$$

$$\frac{\partial}{\partial x_j}(U_j \varepsilon) = \frac{\partial}{\partial x_j}\left[\frac{\upsilon_t}{\sigma_\varepsilon}\frac{\partial \varepsilon}{\partial x_j}\right] + \frac{\varepsilon}{k}(C_{\varepsilon 1}P_k - C_{\varepsilon 2}\varepsilon) \tag{A6}$$

where P_k is the generation rate of turbulent kinetic energy obtained from

$$P_k = -\overline{u_i u_j}\frac{\partial U_i}{\partial x_j} \tag{A7}$$

Table 2 Empirical constants for the k-ε turbulence model

C_μ	$C_{\varepsilon 1}$	$C_{\varepsilon 2}$	σ_k	σ_ε
0.09	1.44	1.92	1.0	1.3

Table 3 Empirical constants for the *k*-ω turbulence model

β'	α	β	σ_k	σ_ω
0.09	5/9	0.075	2	2.0

The value of constants $C_\mu, C_{\varepsilon 1}, C_{\varepsilon 2}, \sigma_k$, and σ_ε are given in Table 2.

A.2.2 Low-Re *k*-ω Turbulence Model. In the low-Re k-ω turbulence model, developed by Wilcox [13], the unknown Reynolds stress tensor, $-\rho\overline{u_i u_j}$, is calculated from Eq. (A3). The turbulent viscosity is obtained from the relation

$$\upsilon_t = \frac{k}{\omega} \tag{A8}$$

To obtain υ_t, two transport equations, one for the turbulent kinetic energy, k, and one for the turbulent frequency, ω, are solved. The transport equations for k and ω equations are, respectively, written as

$$\frac{\partial}{\partial x_j}(U_j k) = \frac{\partial}{\partial x_j}\left[\left(\upsilon + \frac{\upsilon_t}{\sigma_k}\right)\frac{\partial k}{\partial x_j}\right] + P_k - \beta' k\omega \tag{A9}$$

$$\frac{\partial}{\partial x_j}(U_j \omega) = \frac{\partial}{\partial x_j}\left[\left(\upsilon + \frac{\upsilon_t}{\sigma_\omega}\right)\frac{\partial \omega}{\partial x_j}\right] + \alpha\frac{\omega}{k}P_k - \beta\omega^2 \tag{A10}$$

where constants $\beta', \alpha, \beta, \sigma_k$, and σ_ω are given in Table 3.

One of the advantages of k-ω turbulence model is the near wall treatment for low-Re computations. The k-ω model does not involve the complex nonlinear damping functions required in the low k-ε model and is therefore more robust. A low-Re, k-ε model would typically require a near wall resolution of $y^+ < 0.2$, while a low-Re number k-ω model would require the first grid node to be at least $y^+ < 2$. In turbomachinery flows, even $y^+ < 2$ cannot be guaranteed, and for this reason, a new near wall treatment was developed for the k-ω models. It allows for smooth shift from k-ω model to a wall function formulation regarding local y^+ value.

A.2.3 SST Turbulence Model. The SST turbulence model combines the advantages of the k-ω and the k-ε models. The main problem with the k-ω model is its well known strong sensitivity to free stream conditions [14]. Depending on the value specified for ω at the inlet, a significant variation in the results of the model can be obtained. This is undesirable and in order to solve the problem, a blending between the k-ω model near the surface and the k-ε model in the outer region was developed by Menter [15]. It consists of a transformation of the k-ε model to a k-ω formulation and a subsequent addition of the corresponding equations. The k-ω model is thereby multiplied by a blending function F_1 and the transformed k-ε model by a function $1 - F_1 \cdot F_1$ is equal to one near the surface and decreases to a value of zero outside the boundary layer, that is, a function of the wall distance. At the boundary layer edge and outside the boundary layer, the standard k-ε model is therefore recovered

$$F_1 = \tanh\left(\arg_1^4\right) \tag{A11}$$

with

$$\arg_1 = \min\left(\max\left(\frac{\sqrt{k}}{\beta'\omega y}, \frac{500\upsilon}{y^2\omega}\right), \frac{4\rho k}{CD_{k\omega}\sigma_{\omega 2} y^2}\right) \tag{A12}$$

where y is the distance to the nearest wall, and

$$CD_{k\omega} = \max\left(2\rho\frac{1}{\sigma_{\omega 2}\omega}\frac{\partial k}{\partial x_j}\frac{\partial \omega}{\partial x_j}, 1.0 \times 10^{-10}\right) \tag{A13}$$

The SST model accounts for the transport of the turbulent shear stress and is expected to give highly accurate predictions of the onset and the amount of flow separation under adverse pressure gradients. The formulation of the eddy-viscosity

$$\upsilon_t = \frac{\alpha_1 k}{\max(\alpha_1\omega, SF_2)} \tag{A14}$$

where S is an invariant measure of the strain rate. F_2 is a blending function, which restricts the limiter to the wall boundary layer, as the underlying assumptions are not correct for free shear flows

$$F_2 = \tanh\left(\arg_2^2\right) \tag{A15}$$

where

$$\arg_2 = \max\left(\frac{2\sqrt{k}}{\beta'\omega y}, \frac{500\upsilon}{y^2\omega}\right) \tag{A16}$$

References

[1] Gulich, J. E., and Favre, J. N., 1997, "An Assessment of Pump Impeller Performance Predictions by 3D Navier–Stokes Calculations," 3rd ASME Pumping Machinery Symposium, Vancouver, BC, Canada, June 22–26.
[2] Kelder, J. D. H., Dijkers, R. J. H., Van Esch, B. P. M., and Kruyt, N. P., 2001, "Experimental and Theoretical Study of the Flow in the Volute of a Low Specific-Speed Pump," J. Fluid Dyn. Res., **28**(4), pp. 267–280.
[3] Feng, J., Benra, F. K., and Dohmen, H. J., 2010, "Application of Different Turbulence Models in Unsteady Flow Simulations of Radial Diffuser Pump," Forsch. Ingenieurwes., **74**(3), pp. 123–133.
[4] Cheah, K. W., Lee, T. S., Winoto, S. H., and Zhao, Z. H., 2008, "Numerical Analysis of Impeller–Volute Tongue Interaction and Unsteady Fluid Flow in a Centrifugal Pump," 4th International Symposium of Fluids Machinery and Fluid Engineering, Beijing, China, Nov. 24–27, pp. 24–27.
[5] Gonzalez, J. J., Fernandez, J., Blanco, E., and Santolaria, C., 2002, "Numerical Simulation of the Dynamic Effects Due to Impeller Volute Interaction in a Centrifugal Pump," ASME J. Fluid Eng., **124**(2), pp. 348–355.
[6] Spence, R., and Amaral-Texeira, J., 2009, "A CFD Parametric Study of Geometrical Variations on the Pressure Pulsations and Performance Characteristics of Centrifugal Pump," Comput. Fluids, **38**(6), pp. 1243–1257.
[7] Jafarzadeh, B., Hajari, A., Alishahi, M. M., and Akbari, M. H., 2011, "The Flow Simulation of Low-Specific-Speed High-Speed Centrifugal Pump," J. Appl. Math. Modell., **35**(1), pp. 242–249.
[8] Yang, S., Kong, F., and Chen, B., 2011, "Research on Pump Volute Design Method Using CFD," Int. J. Rotating Machinery, **2011**, p. 137860.
[9] Torabi, R., and Nourbakhsh, S. A., 2011, "Hydrodynamic Design of the Volute of a Centrifugal Pump Using CFD," ASME-JSME-KSME Joint Fluids Engineering Conference, Hamamatsu, Shizuoka, Japan, July 24–29, pp. 423–427.
[10] Spence, R., and Amaral-Texeira, J., 2008, "Investigation Into Pressure Pulsations in a Centrifugal Pump Using Numerical Methods Supported by Industrial Tests," Comput. Fluids, **37**(6), pp. 690–704.
[11] Stepanoff, A. J., 1957, *Centrifugal and Axial Flow Pumps*, Wiley, New York.
[12] Pfleiderer, C., 1949, *Centrifugal Pump for Liquids and Gases*, Springer, Berlin, Germany.
[13] Wilcox, D. C., 1986, "Multiscale Model for Turbulent Flows," AIAA 24th Aerospace Sciences Meeting, Reno, NV, Jan. 6–9, AIAA Paper No. 86-0029.
[14] Menter, F. R., 1993, "Multiscale Model for Turbulent Flows," 24th Fluid Dynamics Conference, Orlando, FL, July 6–9, pp. 1311–1320.
[15] Menter, F. R., 1994, "Two-Equation Eddy-Viscosity Turbulence Models for Engineering Applications," AIAA J., **32**(8), pp. 1598–1606.